Disorder controlled hole transport in MEH-PPV

Anto Regis Inigo,[1] Hsiang-Chih Chiu,[1] Wunshain Fann,[1] Ying-Sheng Huang,[2] U-Ser Jeng,[3] Tsang-Lang Lin,[4] Chia-Hung Hsu,[3] Kang-Yung Peng,[5] and Show-An Chen[5]

[1]*Institute of Atomic and Molecular Sciences, Academia Sinica, and Department of Physics, and Institute of Polymer Science and Engineering, National Taiwan University, P.O. Box 23-166, Taipei, Taiwan, Republic of China*

[2]*Department of Electronic Engineering, National Taiwan University of Science and Technology, Taipei 106, Taiwan, Republic of China*

[3]*National Synchrotron Radiation Research Center, Hsinchu 300 Taiwan, Republic of China*

[4]*Department of Engineering and System Science, National Tsing Hua University, Hsinchu 300, Taiwan, Republic of China*

[5]*Department of Chemical Engineering, National Tsing-Hua University, Hsinchu 300, Taiwan, Republic of China*

(Received 20 March 2003; revised manuscript received 14 July 2003; published 2 February 2004)

We analyze the correlation between nanostructure and charge transport in poly(2-methoxy,5-(2′ethyl-hexyloxy)-*p*-phenylene vinylene) (MEH-PPV) films. The MEH-PPV films prepared in toluene (TL) as well as chlorobenzene (CB) solvents were investigated using the time-of-flight method and x-ray scattering. Nondispersive hole transport was observed at room temperature in devices prepared from both solutions. The field and temperature-dependent mobility were analyzed by the Gaussian disorder transport model. The positional disorder parameter in CB is larger than that in TL films. Both energy and position disorders affect the transport property in the devices from CB whereas only energy disorder affects this property in devices from TL. Correspondingly, according to the x-ray scattering measurements, the TL-cast films have larger chain-packed domains and less order-disorder transition interfaces than those for CB-cast films, along the surface normal, i.e., the charge transport direction.

DOI: 10.1103/PhysRevB.69.075201 PACS number(s): 61.41.+e, 73.61.Ph, 61.10.Eq

I. INTRODUCTION

Organic electroluminescent conjugated polymers are technologically important materials for display applications because of the ease of processing and flexibility in synthesis. Fundamentally, they represent a new class of materials in which charge carrier transport between closely packed electronically active chromophores, deserving further understanding. Poly *p*-phenylene vinylene (PPV) and its soluble derivatives have excellent luminescent properties.[1–4] Extensive studies about the morphology and photophysics of the films have been documented in the literature, however, with less work on the charge transport studies. The relationship between the charge transport and the morphology[5,6] is important in the design of light-emitting diodes (LED's), lasers,[7] and transitors.[8] The change in photophysical properties depending on the processing conditions results in the change in the efficiency of the LED's.[9–12]

In luminescent conjugated polymer films, charge transport is governed by hopping processes and mobility can be measured by the time-of-flight (TOF) method. In TOF measurements, a sheet of charge carriers produced by a short nanosecond light pulse moves through the material under the influence of an externally applied voltage and departs the material at the transit time, t_τ, with a mobility $\mu = L/t_\tau E$, where L is the thickness of the sample and E is the externally applied electric field.[13] For carriers moving with constant velocity, the ideal photocurrent transients from the TOF method resemble rectangular shapes. The dispersion of the carrier velocity and traps states will cause the actual photocurrent transients deviating from the ideal shapes. This feature in the photocurrent transient provides microscopic information about charge transports.

The electric field and temperature-dependent mobility have been an intense subject of research. In polymers and organic molecules, the mobility generally follows the Poole-Frenkel behavior,

$$\ln[\mu(E)/\mu_{E=0}] = SE^{1/2}, \tag{1}$$

where E is an externally applied electric field, S is the slope of the field-dependent mobility, and $\mu_{E=0}$ is the zero-field mobility. A powerful method to analyze nondispersive charge transport in organic materials is the Gaussian disorder transport model (GDM) proposed by Bässler and co-workers.[14,15] In the GDM, charge carrier movements through the materials are simulated by hopping between transporting sites on a cubic lattice with fixed distance. Two important parameters in the GDM model are energy σ and position disorder Σ. The energy disorder parameter describes the spread of energy levels associated with transport. The position disorder parameter describes the fluctuation of intersite distance and coupling between sites. It is natural to expect that material morphology can strongly influence σ and Σ. For a given chemical structure, these parameters might depend on processing conditions, temperature treatment, and the solvent used to prepare films. Note that there are extensive publications using the Scher-Montroll continuous-time random-walk model to analyze dispersive transport.[16,17] Because we are observing nondispersive transport, we use Gaussian model to analyze experimental results.

Original and modified versions of GDM's have been applied extensively on variety of polymers and molecularly doped polymers to understand how material properties affect transport. For example, the modified GDM was used to describe molecularly doped polymers with lower doping concentration.[18,19] In these materials the charge carrier mobility is influenced by the presence of the charge-dipole

interaction.[20–22] The dipole moment can be easily measured to correlate the observed property changes. Fewer attempts have been made to correlate charge carrier mobility with the packing of charge-transporting molecules. One of the efforts includes addition of charge-transporting molecules in materials such as poly(styrene), with doping concentration controlling the intersite distance.[23] Alternatively, the hopping-site distance can be modified by the chemical structure of the molecules.[24] Both approaches provide straightforward methods to identify the nature of packing. Conjugated polymers provide different kinds of challenges due to close packing of the charge-transporting sites.[25]

The morphology of MEH-PPV (noncrystalline material) is well known to be sensitive to processing conditions. A considerable amount of work has been reported on the packing conformations of the polymer chains in different solvents. It was found that the packing structure of MEH-PPV in solutions might transfer to the films.[26–28] In this paper we address the hole transport properties of MEH-PPV films and their connection to the film morphology controlled by solvents [toluene (TL) and chlorobenzene (CB)] used to cast the thin films. The positional parameter obtained from the GDM is consistent with film morphology measured by x-ray scattering. The present work attempts to connect structure properties with parameters in Gaussian disorder model. We show the clear correspondence between the position disorder parameter obtained from the GDM and the structure of the films characterized by x-ray scattering. The merit of using the x-ray scattering technique for direct structural information of MEH-PPV films cast from different solvents has been realized earlier by, for instance, Yang *et al.*[29]

II. EXPERIMENTAL METHODS

MEH-PPV solutions of 5 mg/cm^3 in CB and TL were used to prepare thick films on a precleaned ITO (indium tin oxide)-coated glass substrates. The top gold electrodes were deposited using a thermal evaporator. Devices were prepared from two different solution batches. The detailed procedure of device preparation and TOF instrumentation was described in a previous publication.[6] The nascent polymers were characterized by tetrahedral defect and molecular weight measurements. The tetrahedral defect density obtained from the NMR measurements was ~2%. A molecular weight of ~250 000 and polydispersity of 6.5 were obtained from gel permeation chromatography measurements. Recent studies show that the mobility and the type of transport (viz., dispersive or nondispersive) vary with defect concentrations and molecular weights of polymer samples.[8,30] Since charge transport in conjugated polymer films can be affected by either variation of conjugation length or morphology, all films used in the present study were prepared from the same sample batch to minimize the variation in conjugation length. Therefore, the differences in the charge transport observed for the TL or CB sample thin films are attributed mainly to the solvent-dependent film morphology.

Photoluminescence spectra were recorded by a spectrofluorometer (Spex Fluorolog-3). The x-ray reflectivity for films on ITO-coated glass substrate was conducted on an eight-circle diffractometer in the National Synchrotron Radiation Research Center (NSRRC), Taiwan. The x-ray beam, monochromated to 1.5 Å, was collimated into a beam size of 0.25 mm height and 0.4 mm wide at the sample position by two sets of slits separated in 1 m apart. Small-angle x-ray scattering SAXS, measurements were performed on the 8-m SAXS instrument at Tsing-Hua University, Taiwan, with the film surfaces being either perpendicular or parallel to the beam. For the SAXS measurement we detached the sample thin films from glass substrates. The detached films were then carefully folded into thick layers ~120 μm thick and

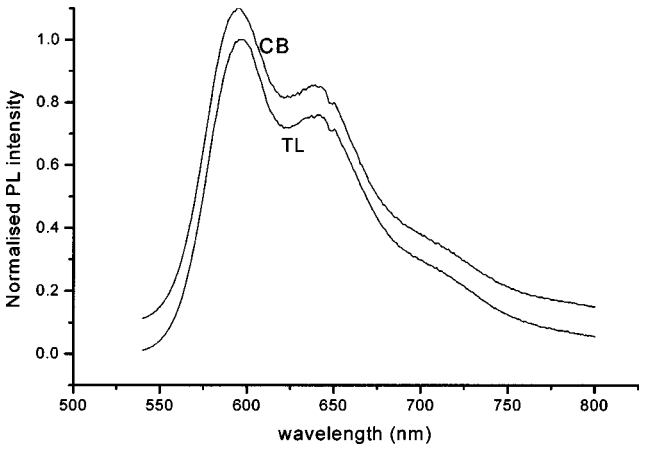

FIG. 1. The PL emission spectrum of MEH-PPV excited at 520 nm for device prepared from (a) TL and (b) CB solutions. Spectra are offset vertically for clarity.

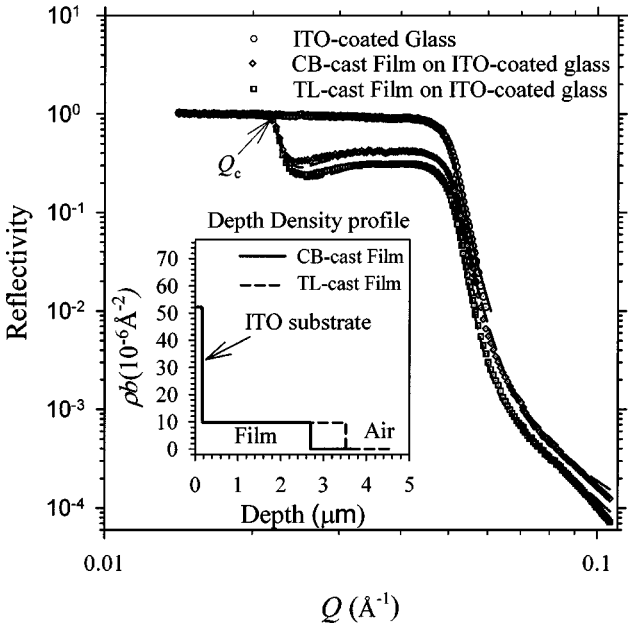

FIG. 2. X-ray reflectivity data for the toluene (TL) cast (squares) and chlorobenzene (CB) cast (diamonds) films of MEH-PPV. Both sets of data are fitted (dashed curve) using the scattering-length-density profiles shown in the inset, respectively. Also shown are the reflectivity data (circles) and the fitting result (solid curve) for the ITO-coated glass substrate for identifying the critical wave vector of the ITO-coated layer at $Q_c \approx 0.04$ Å^{-1}.

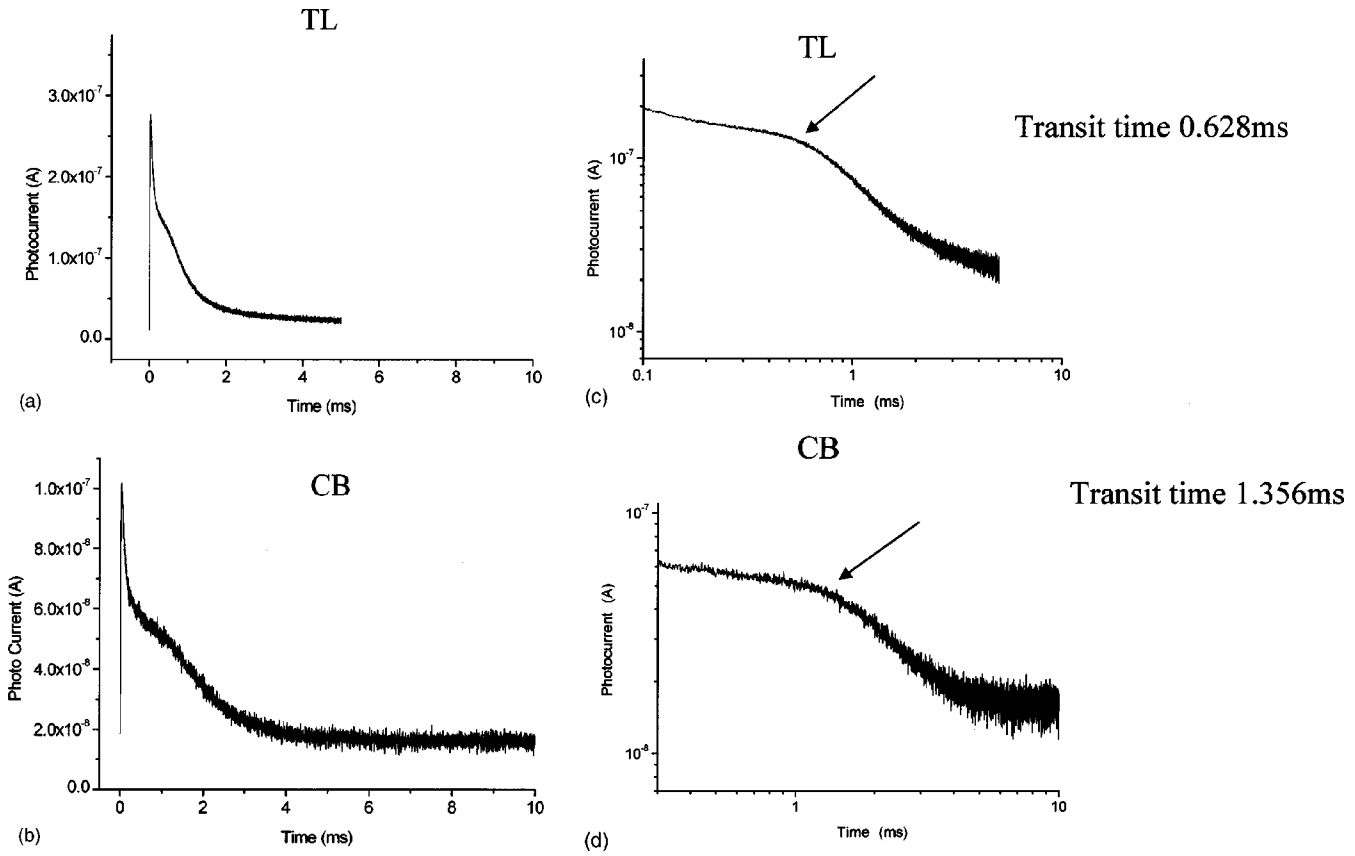

FIG. 3. The photocurrent transients in (a) linear scale and (b) at log-log scale (the arrow points the transit time) at room temperature for films prepared in TL and in CB solutions. The electric field is 1×10^5 V/cm. Both films have thickness of 3.7 μm.

$\sim$5 m$\times$5 mm dimensions. The in-house SAXS instrument uses an 18-kW rotating-anode x-ray source of a copper target. After monochromatization by a graphite crystal, the x-ray was collimated into a pencil-like beam of 1 mm diameter by a there-pinhole collimating system. With a beam wavelength of 1.54 Å and a sample-to-detector distance of 3.8 m, the SAXS instrument scanned the Q range between 0.008 and 0.2 Å^{-1} where $Q=4\pi\sin(\theta/2)/\lambda$ is defined by the scattering angle θ and the wavelength λ of the radiation quanta. A two-dimensional multiwired area detector was used to record the data. The x-ray results presented here are corrected for sample transmission, background, and detector sensitivity and normalized to an absolute scattering scale by comparison with a standard sample of polyethylene. The absolute scattering scale calibration makes the intensity comparison between different sample geometries more reliable.

III. EXPERIMENTAL RESULTS AND ANALYSIS

The fluorescence spectra of the drop-casted films are shown in Fig. 1 for samples from (a) TL and (b) CB. There seems to be less aggregation in films drop-casting from both solvents, judging from the relative weak 650-nm band in the photoluminescence (PL) spectrum.[9] Moreover, there is no significant difference in PL spectra of films from different solvents. The x-ray reflectivity data for the TL- and CB-cast films are shown in Fig. 2. Both samples exhibit the same critical wave vector for total reflection at $Q_c\approx0.022$ and 0.04 Å^{-1}. The smaller critical wave vector indicates that films cast from different solvents have the same density, since $Q_c=(4\pi\rho b)^{1/2}$. Here ρb is the scattering length density determined by the density ρ of the film and the molecular scattering length b for x rays. The same second critical wave vector at $Q_c\approx0.04$ Å^{-1} reflects the ITO-coated layer of the glass substrate. The drop of reflectivity from unity between the two critical wave vectors is due to the beam absorption upon traversing the films. The slightly higher reflectivity profile for the CB-cast film is due to smaller beam absorption, thus a smaller film thickness than the TL-cast film. To extract detailed structural information of the films from the reflectivity data, we used a standard model-fitting algorithm for multiplayer structures. This model considers a continuous transition between successive layers of different ρb, accounted for by a Debye-Waller-like factor.[31]

The beam absorption effect was also taken into account in the fitting algorithm, using a film density of 1.06 g/cm^3 and x-ray linear absorption $\lambda_i=4.83$ cm^{-1} (for 1.5-Å x rays) calculated from the total reflection wave vector of the film. In fact, both sets of data can be fitted (solid curves) with a model of a thick MEH-PPV layer sitting on the ITO-coated glass substrate, using the same scattering-length density (see the inset of Fig. 2), with a thickness of 2.6 μm for the CB-cast film and 3.5 μm for the TL-cast film, respectively. The result shows that the depth density profiles of the MEH-PPV films are independent of the cast solvent used. The smooth-

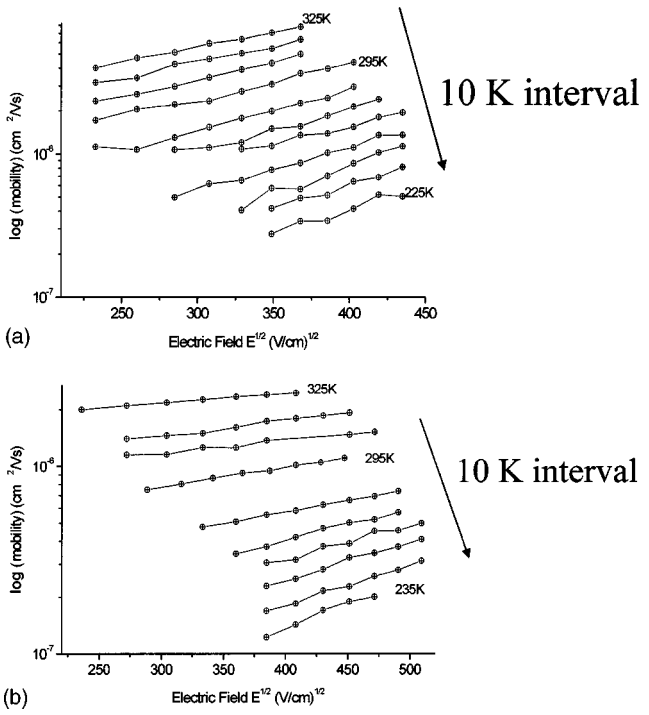

FIG. 4. The field dependent mobility at different temperatures starting from 225 to 335 K at the interval of 10 K for devices prepared from (a) TL and (b) CB.

ness of the scattering-length-density profiles (or density profiles along depth direction) obtained from the x-ray reflectivity data clearly demonstrates the high homogeneity (averaged in the in-plane direction) across the films.

Figure 3(a) shows the linear TOF transient plots for both TL and CB devices with a film thickness of 3.7 μm. The well-defined plateau in linear TOF transient plots demonstrates the high qualities of the samples. At room temperature, the TOF transients exhibit a spike at the beginning, followed by a plateau and finally a long tail, indicating a nondispersive behavior. The initial spike is due to the *RC* time constant of the apparatus. The transit time was determined from the log*i*-log*t* plot by crossing of the asymptotes to the plateau and the declining slope, shown in Fig. 3(b). The field and temperature ranges from which mobility can be extracted from TOF current transits depend upon several factors. The Signal-to-noise ratio limits the mobility measurements at low fields and low temperatures. The time resolution of the circuit, limited by *RC* time constant of the circuit, limits the high-temperature mobility measurement. Finally dielectric breakdown sets the limit for high-field measurements. For temperatures lower than 225 K, the transport becomes so highly dispersive such that the deduction of transit time by the log*i*-log*t* plot becomes unreliable. Figure 4 shows the field-dependent mobility from 225 to 325 K at intervals of 10 K for devices prepared from (a) TL and (b) CB. The mobility of the TL devices is higher than that for the CB devices. Throughout the temperature range investigated here, the mobility follows the Poole-Frenkel relationship, Eq. (1). The slope S of the field-dependent mobility and the zero-field mobility $\mu_{E=0}$ in Eq. (1) are calculated for further analysis. The energy disorder parameter (in meV) is determined by the zero-field mobility using the following relationship (see Fig. 5),

$$\mu_{(E=0)} = \mu_0 \exp[-(T_0/T)^2], \tag{2}$$

where μ_0 is the mobility at infinite temperature and T_0 is a characteristic temperature of the material. The energy disorder parameter σ, which is the width of Gaussian density of states, is related to T_0 as $T_0 = 2\sigma/3k$, where k is the Boltzmann constant. Figure 5 shows the $\ln \mu_{(E=0)}$ vs $1/T^2$ plot for TL and CB films. The energy disorder values for the devices for CB and TL are 92 ± 2 and 63 ± 1 meV, respectively.

The electric-field dependence of the mobility is stronger in TL devices than that in CB devices at room temperature. This is an indication that positional disorder is larger in the CB films for the following reasons.

In the presence of larger positional disorder, charge carriers can diffuse against the direction of the applied field more easily.[14] Because charge carriers can detour around the next energetically favorable charge-transporting site by diffusion, it may travel against the applied field, thus making the mobility smaller. As a result, the dependence of mobility on applied field becomes less prominent as the positional disorder increases.[23] Furthermore, as temperature increases, the slope of the field-dependent mobility decreases for materials with large positional disorder. This is because the thermal energy of charge carriers increases as the diffusion process becomes more prominent at high temperature. This behavior is observed in the CB devices, where Fig. 4(b) shows that the slope S gradually decreases as the temperature increases. On the other hand, the slope of the field-dependent mobility of TL devices depends weakly on temperature [Fig. 4(a)]. De-

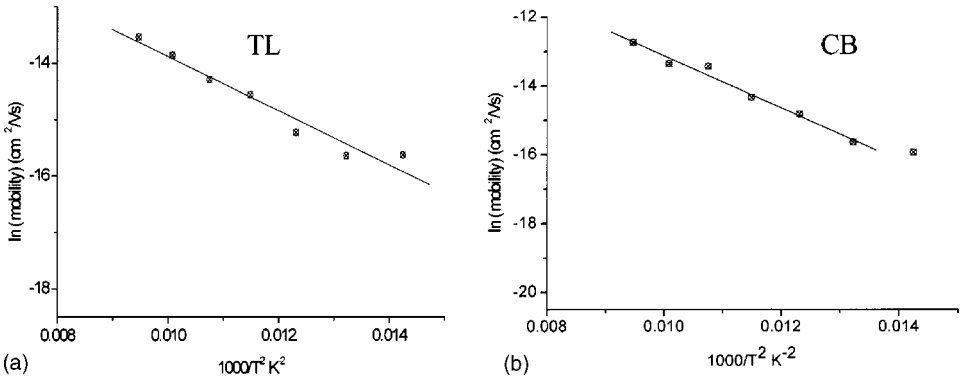

FIG. 5. The zero field mobility is plotted against $1/T^2$ for devices prepared from (a) TL and (b) CB to determine energy disorder parameter.

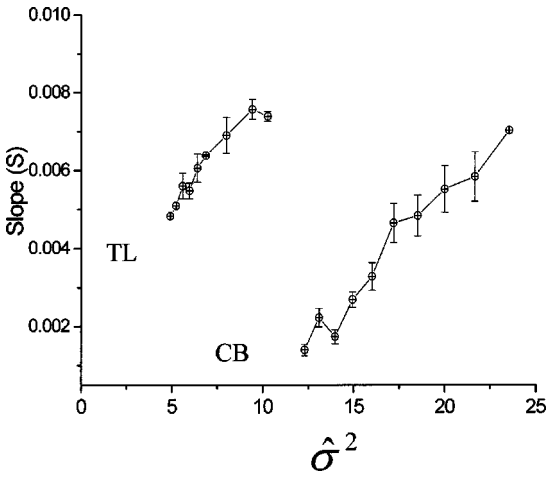

FIG. 6. The slope (S) at different temperatures is plotted against $\hat{\sigma}^2$ for devices prepared from TL and CB to determine position disorder parameter.

vices made from TL films have larger S values, i.e., mobility increases more rapidly with the applied field at all temperatures.

The actual value of the positional disorder parameter is obtained by plotting the slope (S) obtained for various temperatures against $\hat{\sigma}^2$, where $\hat{\sigma}^2=(\sigma/kT)^2$. The results are shown in Fig. 6. The position disorder parameter is 10 ± 1 for CB and less than 1.5 for TL films. For the CB film, S decreases rapidly as the temperature increases from 225 to 325 K. This is characteristic of disordered semiconductors, where the position disorder is important as discussed in the preceding paragraph. The mobility is also less sensitive to electric field in the CB film, another characteristic of geometrical disorder. On the other hand, the strong dependence of S values on temperature is not observed in TL films. Hence the hole transport in the TL film is mainly affected by energy disorder, while the charge transport is governed by both energy and position disorder in CB devices.

Although there was no significant difference in the PL spectra, field- and temperature-dependent hole transport is different for CB and TL films. These results show that subtle changes in morphology related to charge transport do not have any effect on the PL emission. However, the x-ray scattering results do exhibit different morphology. While the x-ray reflectivity data shown previously reveal very much the same depth-density profiles (averaged over in-plane structures) for the CB and TL films, the SAXS result clearly demonstrates different local structural characteristics for the CB and TL films, as detailed below.

The two-dimensional SAXS patterns obtained with x rays parallel and perpendicular to the CB film surface are shown in Figs. 7(a) and 7(b), respectively. With the incident beam being nearly parallel to the film, the SAXS measured [Fig. 7(a)] shows an impressive uniaxial symmetry in the direction perpendicular to the film surface. The TL film also exhibits similar results. The pattern indicates a larger amount of local structural inhomogeneity (aggregates or chain-packed domains) existing along the depth direction of the film. On the other hand, the SAXS pattern with the beam perpendicular to

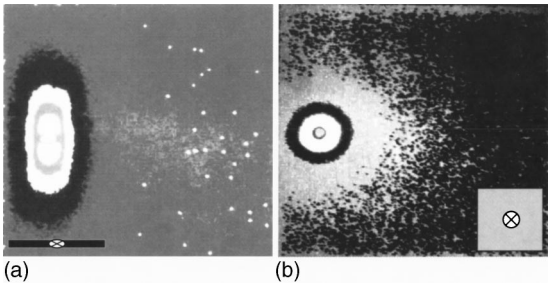

FIG. 7. (a) SAXS pattern for the free-standing film of MEH-PPV, measured with a beam parallel to the film surface. The black rectangle indicates the film orientation, whereas the cross indicates the incident direction. The vertical strong scattering axis seen corresponds to the depth structural information of the film. (b). SAXS pattern for the free-standing film (square) of MEH-PPV, measured with a normal incident beam (cross).

the film, show a circular isotropic pattern [Fig. 7(b)] for a symmetrical structure in the in-plane direction. Figure 8 shows the SAXS profile of the TL- (circles) and CB- (squares) cast films in the surface normal direction. The one-dimensional I-Q data shown in Fig. 8 were obtained by averaging from the two-dimensional detector pixels of the same Q values along the symmetrical scattering directions. The SAXS profile for the TL film shows the power-law scattering characteristic $I(Q)\propto Q^{-p}$ with $p=4.2$ (long dashed line). On the other hand, the corresponding SAXS profile for the CB film has the power-law behavior of $p=4$ (short dashed line in Fig. 8) in the higher Q region. The CB data then deviate from the power-law behavior for $Q \lesssim 0.02$ Å^{-1}. In the fractal model, scattering dominated by a fractal surface morphology is described by $I(Q)\propto Q^{-(6-D_s)}$ with the surface fractal dimension D_s between 2 and 3.[32] For an extreme limit of the flat surface with $D_s=2$, the fractal scattering degenerates into the Porod law of $I(Q)\propto Q^{-4}$. A slightly larger p than four indicates rougher interfaces.[33] As

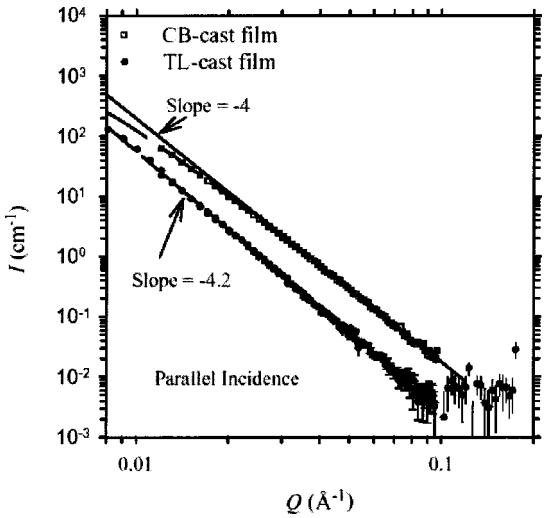

FIG. 8. SAXS profiles along the surface normal direction for the TL (circles) and CB (squares) cast MEH-PPV films, under a parallel incident beam. The data are fitted by the power-law scattering with $p=-4.2$ and -4.0 (solid and dashed lines) for the respective film.

Q decreases, the surface scattering behavior gradually transits to the mass or fractal mass scattering $I(Q) \propto Q^{-D_m}$, with the mass fractal dimension (equal to the scattering power p) $D_m \leqslant 3$. The size R of the fractal facets of a scattering entity then can be estimated from $R \sim 1/Q_f$. Here, Q_f is a crossover point in the transition of scattering behavior from the surface fractal to the mass fractal. According to the fractal model, the interfaces for the CB-cast film between the ordered and disordered domains are smoother ($p=4$) than that for the TL-cast film ($p=4.2$), reflecting a better orientation of the aromatic rings of MEH-PPV along the film plane in the CB-cast film. Unfortunately, in the Q range studied, we could not observe the transition from the surface scattering to the mass scattering for both films. Thus, we have difficulty in determining the size of the secondary ordered domains for the films using the fractal model. Nevertheless, the earlier departure of the CB data from the surface scattering characteristics indicates a smaller domain size or correlation length in the depth direction for the CB-cast film, in comparison with the TL-cast film.

Furthermore, the surface fractal scattering intensity relates to the total interfacial area and the scattering contrast at the interfaces.[34] The significantly higher surface scattering intensity ($Q > 0.02$ Å^{-1}) of the CB-cast film implies more interfacial area orientation in the direction parallel to the film surface. Here, we have assumed the scattering contrast at the transition interfaces of the order and disorder domains in both films is similar. This assumption may not be far off from the reality, since both films have similar depth density profiles, as revealed by the x-ray reflectivity measurement discussed previously. In comparison with the TL-cast film, the smaller ordered domains with more ordered-disordered transition interfaces across the CB film may discourage charges more in traversing the film. We feel that the denser distribution of the order-disorder transition interfaces, which discourages the charge transport more, should correspond to the larger position disorder parameter of a larger diffuse effect observed in the CB film.

IV. DISCUSSION

In this study, we have found the charge transport of the conjugate polymer films relates delicately to the local packing characteristics of the MEH-PPV molecules. Since the solvents used for casting the films affect the final structural morphology of conjugated polymer networks and thus the charge transport, the microscopic mechanism of the structural evolution of MEH-PPV from solution to final cast films deserves further discussion. Most likely, the solution structure of MEH-PPV can be kinetically trapped in the nonequilibrium drop-cast films, resulting in the observed solvent-dependent structure and consequently the solvent-dependent transport property. Indeed, the small-angle neutron scattering[35] result for the solution structures of MEH-PPV shows that MEH-PPV in TL and CB have the same power-law scattering of $I(Q) \sim Q^{-p}$ with $p=1$, indicating a similar rigid local interchain packing for MEH-PPV in both solutions.[36] On the other hand, Nguyen, Doan, and Schwartz[28] reported a significantly larger radius of gyration for MEH-PPV in CB than that in TL. These solution-dependent structure characteristics for MEH-PPV may be trapped in the films to a certain degree and may relate closely to the differences in the structure features observed in the CB- and TL-cast films.

Here, we emphasize the correlation between the structural information and the charge transport for the MEH-PPV films. For local structure, the SAXS data shown in Fig. 8 indicates that the CB film has smaller ordered (chain-packed) domains and more order-disorder (chain-not-packed) transition interfaces than the TL film along the vertical direction. Thus the distance fluctuation between hopping sites is larger in CB films, which corresponds to large positional disorder, according to the GDM. This is consistent with our charge transport result, where we have a much larger position disorder for the CB film. Despite the differences in the local structure observed directly by SAXS or indirectly by the TOF measurement, both films have a similar global homogeneous morphology, as revealed by the x-ray reflectivity data.

A general method to describe morphology in luminescent conjugated polymers is through the terms *aggregation* and *nonaggregation*, which has been widely used to explain the change in the photophysical properties of conjugated polymers. *Aggregation* means the overlap of wave functions of one or more chromophores in the same chain or different chains of the polymer molecule. The effect of aggregation can be observed from optical spectroscopic methods such as PL spectra or by scanning near-field optical microscopy.[37] In aggregates, it is generally argued that the emission essentially comes from the overlap of π orbitals between two adjacent chromophores, which may be from same chain or from the neighboring chains, separated by less than 1 nm. Consequently a change in distribution of the alignment or orientation of the polymer chains in longer length scale will affect the charge transport but may not influence the overall luminescence of the material.

The results in the present work show that structural features influence the transport property more than that of the aggregates and nonaggregates found in the PL spectrum. The evidence for this comes from Fig. 1, since there is no significant change in the PL spectra of the devices from CB and TL devices. The charge transport property is characterized or affected by the presence of long-range ordering in polymer samples prepared from different solvents. Charge transport of the films relates to the hopping of charge carriers (or the overlap of π-orbitals) within and between the ordered (chain-packed) and nonordered regions (chain-relaxed) in the films. Therefore the size and distribution of the ordered regions, influencing the hopping rate and its dispersion, can be decisive in the nondispersive charge transport observed for the MEH-PPV films cast from CB and TL.

The situation here is very much different from the attempts to understand the effects of geometric disorder on mobility by doping materials with charge-transporting sites in poly(styrene) matrix.[23] In poly(styrene), the dopant molecules tend to form clusters and the intersite distances are somewhat defined in the entire polymer matrix. Monte Carlo simulations can be performed by considering the charge hopping from the center of the one cluster to another.[18] In MEH-

PPV, both regions viz., ordered (closely packed) and nonordered (loosely packed) regions have transporting sites participating in the charge transport processes. The intersite distances for the hopping of the charge carriers may be small inside the ordered regions and larger in nonordered regions. Although the Bässler's phenomenological disorder model provides a useful starting framework for theoretical understanding, the model does not take into account sample inhomogeneity. Only spatial-averaged energy and position disorder parameters in the materials can be obtained from the model. Rakhamanova and Conwell took the first step to include inhomogeneity in energy disorder theoretically.[38] Their model incorporated energy disorder 120 meV in some part of the material, and 80 meV in the other part. The simulation indicated a decreased mobility by a factor of 10. The zero field mobility followed Arrenhius ($\ln \mu \propto 1/T$) rather than the non-Arrenhius form ($\ln \mu \propto 1/T^2$). These authors concluded that the activated behavior was due to the inhomogeneity. The temperature-dependent mobility in this work cannot distinguish between the $1/T$ and $1/T^2$ behaviors. In addition, the mobility differences from TL and CB devices are not as dramatic as suggested by the model calculation, because in the present study the strong variation is in geometric disorder rather than in energy disorder. Currently, we are working on extension of the work of Rakhamanova and Conwell to include spatial inhomogeneity. This should provide further insight for connection of x-ray measurement and transport model. In addition to the inhomogeneity effect, an extension of the disorder model to include correlation effect might also be essential in applying the disorder model to a larger class of materials.[39]

V. CONCLUSION

In summary, the electronic properties controlled the charge transport in MEH-PPV cannot be fully accessible by optical spectroscopy such as fluorescence measurements. But there exists correlation between TOF and x-ray results. The hole transport in toluene devices is controlled predominantly by the energetic disorder and in CB devices by both energy and position disorder.

ACKNOWLEDGMENTS

This work is supported by National Research Council, Taiwan, Republic of China and MOE Program for Promoting Academic Excellence of Universities under Grant No. 91-E-FA04-2-4A.

[1] J. H. Buroughes, D. D. C. Bradley, A. R. Brown, R. N. Marks, K. Mackey, R. H. Friend, R. L. Burn, and A. B. Holmes, Nature (London) **347**, 539 (1990).
[2] R. H. Friend, R. W. Gymer, A. B. Holmes, J. H. Burroughes, R. N. Marks, C. Taliani, D. D. C. Bradley, D. A. DosSantos, J. L. Bredas, M. Lögdlung, and W. R. Salaneck, Nature (London) **397**, 121 (1999).
[3] S. Forero, P. H. Nguyen, W. Brutting, and M. Schwoerer, Phys. Chem. Chem. Phys. **1**, 1769 (1999).
[4] L. Dai, B. Winkler, L. Dong, and A. W. H. Mau, Adv. Mater. (Weinheim, Ger.) **13**, 915 (2001).
[5] C. H. Tan, A. R. Inigo, W. S. Fann, P. K. Wei, Y. S. Huang, G. Y. Perng, and S. A. Chen, Org. Electron. **3**, 85 (2002).
[6] A. R. Inigo, C. H. Tan, W. S. Fann, Y. S. Huang, G. Y. Perng, and S. A. Chen, Adv. Mater. (Weinheim, Ger.) **13**, 504 (2001).
[7] M. A. D. Garcia, G. Hide, B. J. Schwartz, M. R. Andersson, Q. Pei, and A. J. Heeger, Synth. Met. **84**, 455 (1997).
[8] S. Shaked, S. Tal, Y. Roichman, A. Razin, S. Xiao, Y. Eichen, and N. Tessler, Adv. Mater. (Weinheim, Ger.) **15**, 913 (2003).
[9] Y. Shi, J. Liu, and Y. Yang, J. Appl. Phys. **87**, 4254 (2000).
[10] J. Liu, Y. Shi, L. Ma, and Y. Yang, J. Appl. Phys. **88**, 605 (2000).
[11] T. Q. Nguyen, R. C. Kwong, M. E. Thompson, and B. J. Schwartz, Appl. Phys. Lett. **76**, 2454 (2000).
[12] T. Q. Nguyen, I. B. Martini, J. Liu, and B. J. Schwartz, J. Phys. Chem. B **104**, 237 (2000); R. Jakubiak, C. J. Collison, W. C. Wan, and L. J. Rothberg, J. Phys. Chem. A **103**, 2394 (1999).
[13] W. E. Spear, J. Non-Cryst. Solids **1**, 197 (1969).
[14] H. Bässler, Phys. Status Solidi B **175**, 15 (1993).
[15] P. M. Borsenberger, L. T. Pautmier, and H. Bässler, Phys. Rev. B **46**, 12 145 (1992).
[16] S. Berleb and W. Brütting, Phys. Rev. Lett. **89**, 286601 (2002).
[17] P. W. M. Blom and M. C. J. M. Vissenberg, Phys. Rev. Lett. **80**, 3819 (1998).
[18] B. Hartenstein, H. Bässler, S. Huen, P. Borsenberger, M. V. D. Auweraer, and F. C. D. Schryver, Chem. Phys. **191**, 321 (1995).
[19] R. H. Young and N. G. Rule, Phys. Rev. Lett. **72**, 388 (1994).
[20] D. H. Dunlop, P. E. Parris, and V. M. Kenkre, Phys. Rev. Lett. **77**, 542 (1996).
[21] R. H. Young and J. J. Fitzgerald, J. Chem. Phys. **102**, 6290 (1995). Extensive references are listed in this paper on the charge transport in the dipolar medium by various groups including the work of P. M. Borsenberger and co-workers.
[22] S. V. Novikov, D. H. Dunlop, V. M. Kenkre, P. E. Parris, and A. V. Vannikov, Phys. Rev. Lett. **81**, 4472 (1998).
[23] R. H. Young and J. J. Fitzgerald, J. Chem. Phys. **102**, 9380 (1995); R. H. Young, *ibid.* **103**, 6749 (1995).
[24] H. C. F. Martens, P. W. M. Blom, and H. F. M. Schoo, Phys. Rev. B **61**, 7489 (2000).
[25] P. W. M. Blom and M. C. J. M. Vissenberg, Mater. Sci. Eng., R. **27**, 53 (2000).
[26] J. Yu, D. Hu and P. F. Barbara, Science **289**, 1327 (2000).
[27] C. J. Collision, L. J. Rothberg, V. Treemaneekaran, and Y. Li, Macromolecules **34**, 2346 (2001).
[28] T. Q. Nguyen, V. Doan, and B. J. Schwartz, J. Chem. Phys. **110**, 4068 (1999).
[29] C. Y. Yang, F. Hide, M. A. D. Garcia, A. J. Heeger, and Y. Cao, Polymer **39**, 2299 (1998).
[30] A. R. Inigo, H. C. Chiu, W. S. Fann, Y. S. Huang, U. S. Jeng, C. H. Hsu, K. Y. Peng, and S. A. Chen, Synth. Met. **139**, 581 (2003).
[31] J. F. Anker and C. F. Majkrzak, in *Neutron Optical Devices and*

Applications, edited by C. F. Majkrzak and J. L. Woods [Proc. SPIE **1738**, 260 (1992)].
[32] P. W. Schmidt, D. Avnir, and D. Levy, J. Chem. Phys. **94**, 1474 (1991).
[33] S. Koizumi, M. Annaka, S. Borbely, and D. Schwahn, Physica B **276–278**, 367 (2000).
[34] J. Teixeira, J. Appl. Crystallogr. **21**, 781 (1988).
[35] W.-C. Ou-Yang, H.-L. Chen, D. L. Ho, C.-T. Tsao, G. Yang, K.-Y. Peng, S.-A. Chen, and C. C. Han (private communications).
[36] L. A. Feigin and D. I. Svergun, *Structure Analysis by Small-Angle X-ray and Neutron Scattering* (Plenum, New York, 1987).
[37] T. Q. Nguyen, B. J. Schwartz, R. D. Schaller, J. C. Johnson, L. F. Lee, L. H. Haber, and R. J. Saykally, J. Phys. Chem. **105**, 5153 (2001).
[38] S. V. Rakhmanova and E. M. Conwell, Appl. Phys. Lett. **76**, 3822 (2000).
[39] Y. N. Gartstein and E. M. Conwell, Chem. Phys. Lett. **245**, 351 (1995).